JMEPEG (1999) 8:591-597 

# Influence of Nitrogen in the Shielding Gas on Corrosion Resistance of Duplex Stainless Steel Welds

*R.B. Bhatt, H.S. Kamat, S.K. Ghosal, and P.K. De*

*(Submitted 11 September 1998; in revised form 24 March 1999)*

**The influence of nitrogen in shielding gas on the corrosion resistance of welds of a duplex stainless steel (grade U-50), obtained by gas tungsten arc (GTA) with filler wire, autogenous GTA (bead-on-plate), electron beam welding (EBW), and microplasma techniques, has been evaluated in chloride solutions at 30 °C. Pitting attack has been observed in GTA, electron beam welding, and microplasma welds when welding has been carried out using pure argon as the shielding gas. Gas tungsten arc welding with 5 to 10% nitrogen and 90 to 95% argon, as the shielding gas, has been found to result in an improved pitting corrosion resistance of the weldments of this steel. However, the resistance to pitting of autogenous welds (bead-on-plate) obtained in pure argon as the shielding gas has been observed to remain unaffected. Microscopic examination, electron probe microanalysis (EPMA), and x-ray diffraction studies have revealed that the presence of nitrogen in the shielding gas in the GTA welds not only modifies the microstructure and the austenite to ferrite ratio but also results in a nearly uniform distribution of the various alloying elements, for example, chromium, nickel, and molybdenum among the constituent phases, which are responsible for improved resistance to pitting corrosion.**

**Keywords** Ar-$N_2$ shielding gas, duplex stainless steel, gas tungsten arc welding, pitting corrosion

## 1. Introduction

A new era of duplex stainless steels started when nitrogen was introduced as one of the main alloying elements in these steels. Nitrogen increases the corrosion resistance, especially of the austenite phase. Nitrogen is a strong austenite stabilizer, and it increases the temperature of transformation to austenite (Ref 1). Nitrogen has also been found to accelerate the partial transformation from ferrite to austenite during cooling after welding. In addition, it may help in bringing about homogenization of chromium distribution in the two phases, ferrite and austenite, besides minimizing the extent of microsegregation of melting point depressant alloying/impurity elements. All these factors would result in a significant improvement in the integrity of the welded assembly and its corrosion resistance in particular.

Various investigators have made attempts to improve the corrosion resistance, toughness, and weldability of duplex stainless steels by controlling the composition and austenite to ferrite ratio of the base metal and weld deposits. However, they have recorded wide differences in opinion about the nature of corrosion resistance of welded structures. Redmerski et al. (Ref 2) reported that localized corrosion resistance in simulated sea water of autogenous gas tungsten arc (GTA) weldments of a duplex stainless steel was far inferior to that of its base metal; whereas, for a cast duplex stainless steel of similar composition, other studies (Ref 3) have shown that the corrosion resistance in 10% $FeCl_3$ was the same for the base material and a coated electrode weldment. Pleva and Nordin (Ref 4) have indicated that both filler metal composition and weld microstructure affected the pitting resistance in $FeCl_3$, while Miyuki et al. (Ref 5) have reported that welding conditions (heat input, preheat temperature, and number of phases) for welding Sumitomo DP-3 alloy did not affect the pitting corrosion resistance in synthetic sea water at 80 °C, although the welded samples were found to possess a slightly lower pitting potential than the base metal. The recommendations for optimum welding parameters also differs in literature. Both slower cooling of the weld metal and the heat-affected zone (HAZ) as well as faster cooling to ensure sufficient austenite formation and mechanical strength have been recommended by various investigators (Ref 6). Such differences in the corrosion behavior of welded structures point to the necessity of further development of specific welding parameters/conditions suitable for different grades of duplex stainless steels.

The present trend is to maintain the austenite to ferrite ratio as 1 to 1 or 3 to 2 to increase the weldability to obtain soundness in the welded assembly and the required properties including undiminished corrosion resistance. It is mostly necessary to use filler metal that contains ≥8% nickel for obtaining a weld with similar toughness and corrosion resistance as the base metal. Use of filler metal when GTA and plasma welding thin sheets and making welded thin-walled tubes and pipes is not economically advantageous. Moreover, an increase of austenite with nickel in the filler metal appeared to degrade the weld pitting property through the dilution of the nitrogen content in the austenite (Ref 7).

It has also been observed that weldments of nitrogen containing duplex stainless steels suffer from pitting attack due to loss of nitrogen during welding even with the use of filler metals that contained nitrogen.

The purpose of this investigation was to examine the possibility of introducing nitrogen in GTA weldments of a duplex

**R.B. Bhatt** and **H.S. Kamat,** Advanced Fuel Fabrication Facility, BARC, Tarapur, India; and **S.K. Ghosal** and **P.K. De,** Materials Science Division, Bhabha Atomic Research Centre, Trombay, Mumbai, India. Contact e-mail: pkde@apsara.barc.ernet.in.

stainless steel, U-50, which contained only 0.04% nitrogen, by using nitrogen containing shielding gas to maintain an optimum austenite to ferrite ratio in the weld and to increase the pitting corrosion resistance of such weldments. The weldments thus produced were characterized both in terms of their microstructure and resistance to pitting. The effects of other welding methods, such as autogenous GTA, plasma, and electron beam welding, have also been investigated.

## 2. Experimental

The material used was duplex stainless steel, U-50, mill-annealed, in the form of plate, 3 mm thick. Table 1 gives the chemical composition of this steel, the filler wire used, and one weldment.

Figure 1 shows the joint design for GTA welding. The filler material used was Sandvik wire (1.6 mm diameter) electrode 22-8-3L (Sandvik Steel Company, Scranton, PA). Welds were prepared in single pass using shielding gases that contained (a) pure argon, (b) 5%Ni- 95%Ar, and (c) 10%Ni-90%Ar. To find the effect of other welding methods, bead-on-plate autogenous welds were made using three different welding techniques, namely GTA, electron beam welding (EBW), and microplasma. Table 2 gives the welding parameters associated with the previously mentioned welds. Mixtures of nitrogen and argon as shielding gas were used for the GTA welding of stainless steels. Nitrogen content (Ref 8) in the nitrogen and argon mixture was as high as 20%. For this reason, no difficulties were encountered during experimental as well as production welding operations with 5 to 10% nitrogen in the shielding gas.

Rectangular specimens (25 by 10 by 3 mm) were cut from the welded plate (weld region at the center of the specimen and in the width direction). They were polished with successive grades of emery paper up to 600 grade. The specimens were cleaned thoroughly in double distilled water and acetone before the test exposures. After exposure specimens were examined under optical as well as scanning electron microscopes. Weld microstructures were examined by etching the polished specimens in 10% oxalic acid at 10 V and in 40% KOH at 6 V, electrolytically.

Pitting corrosion resistance of the specimens was studied in 6% $FeCl_3$ solutions at 30 °C for 24 h as per ASTM Standard G 48. Specimens were weighed before and after each exposure to the previously mentioned solution for the measurement of corrosion rate. Initially some tests were carried out to determine the critical pitting temperature in 6% $FeCl_3$ solution as per ASTM Standard G 48, but such tests were discontinued because of ambiguous observations. Samples exposed to the solution in the temperature range of 35 to 45 °C did not show any presence of pits when examined under optical microscope. However, on light polishing using 0.8 μm diamond paste, a large number of pits were visible. Hence, the experiments in 6% $FeCl_3$ solutions were confined to the measurement of change in weight after the exposures.

Pitting potentials were measured by anodic polarization following ASTM Standard G 5 at room temperature. Sodium chloride solutions were used as the test media. The solutions were deaerated by passing purified argon gas before and during each experiment. A scan rate of 50 mV/min was used. One saturated calomel electrode (SCE) was employed as the reference electrode. In order to achieve reproducible results, all potential scans were carried out starting from –1000 mV (SCE) to a few millivolts above the pitting potentials.

The ferrite contents of the welds were measured by x-ray diffraction (XRD) analysis using integrated peak intensity ratio computation. Ferrite estimate by the XRD technique provides accurate (within ±1%) and reproducible results (Ref 9, 10) requiring no calibrated sample; hence it was used in this study. Reference 11 provides a comparison of various techniques of

**Table 1 Nominal composition of U-50, 22-8-3L filler wire, and one weldment**

| | Composition, wt% | | | | | | | | |
|---|---|---|---|---|---|---|---|---|---|
| **Material** | **C** | **Cr** | **Ni** | **Mo** | **Mn** | **N** | **Si** | **P** | **S** |
| U-50 | 0.028 | 20.98 | 6.97 | 2.5 | 1.66 | 0.04 | 0.5 | 0.024 | 0.008 |
| 22-8-3L | 0.02 | 22.5 | 8.0 | 3.0 | 1.6 | 0.14 | 0.5 | 0.02 | 0.02 |
| Weldment in 5%$N_2$-95%Ar shielding gas | 0.025 | 17.9 | 9.3 | 3.1 | 1.7 | 0.12 | 0.5 | 0.02 | 0.02 |

**Table 2 Welding parameters used for the various weldments on 3 mm thick specimens**

| **Welding methods** | **Filler material** | **Current, A** | **Arc voltage** | **Speed, mm/s** | **Flow rate, L/m** | **Heat input, kJ/m** |
|---|---|---|---|---|---|---|
| **Gas tungsten arc** | | | | | | |
| Pure argon | 22-8-3L | 60 | 11 | 1.8 | 12 | 0.36 |
| 5%$N_2$-95%Ar | 22-8-3L | 60 | 11 | 1.8 | 12 | 0.36 |
| 10%$N_2$-90%Ar | 22-8-3L | 60 | 11 | 1.8 | 12 | 0.36 |
| **Autogenous bead-on-plate** | | | | | | |
| Gas tungsten arc (pure argon) | … | 60 | 10 | 2.5 | 10 | 0.24 |
| Microplasma(a) (pure argon) | … | 17 | 20 | 0.66 | … | 0.50 |
| Electron beam welding | … | 0.015 | 60,000 (acceleration voltage) | 2.08 | … | 0.43 |

(a) For microplasma welding, shielding gas pressure and plasma gas pressure were 0.137 and 0.034 MPa, respectively.

ferrite estimation for duplex stainless steels. Concentration profiles of chromium, nickel, and molybdenum in the welds were obtained by electron probe microanalysis (EPMA) in which wavelength dispersive spectrometer was used. The electron beam size used (1.4 μm) was much smaller than the ferrite and the austenite grains and thus small enough to differentiate ferrite from austenite. Chemical composition was measured by the point count technique using profile scan in steps of 5 μm. Optical and scanning electron microscopes were used for microstructural investigations.

## 3. Results

### *3.1 Microstructure*

Figure 2 shows a typical microstructure of mill-annealed, U-50. Elongated bands of austenite and ferrite can be seen in the microstructure, which contains approximately 27% ferrite in an austenite matrix. Hot working at elevated temperatures results in the elongated band structure. Table 3 gives the ferrite contents obtained in the different weldments as measured by XRD analyses.

**Table 3 Ferrite contents in various weldments**

| Material | Filler wire | Ferrite, % |
|---|---|---|
| Base metal | … | 27 |
| Gas tungsten arc welds | | |
| Pure argon | 22-8-3L | 43 |
| 5%$N_2$-95%Ar | 22-8-3L | 35 |
| 10%$N_2$-90%Ar | 22-8-3L | 29 |
| Autogenous bead-on-plate | | |
| Gas tungsten arc | … | 64 |
| Microplasma | … | 73 |
| Electron beam welding | … | 77 |

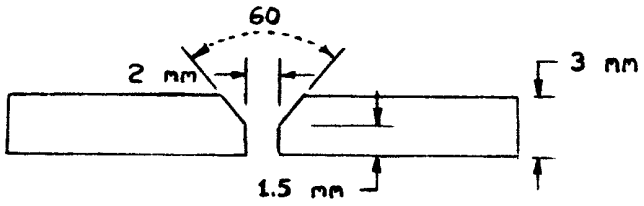


**Fig. 1** Joint design

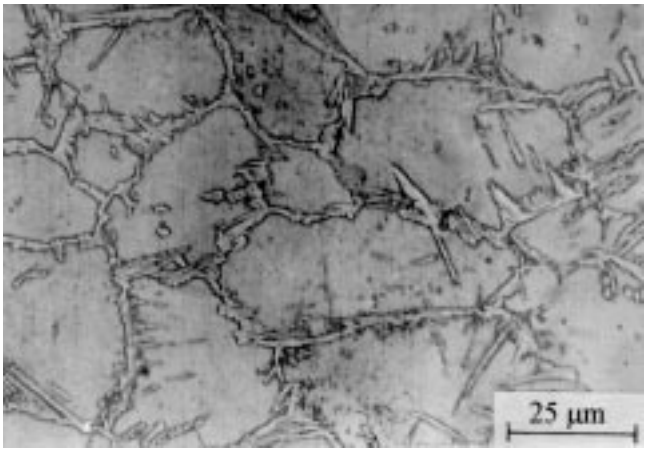


**Fig. 3** Gas tungsten arc weldment microstructure (pure argon)

Welding with filler wire 22-8-3L in the presence of pure argon resulted in an increase in ferrite content to 43% in the weld. Figure 3 shows the weld metal structure, which consisted of mainly ferrite grains with a continuous network of austenite at the ferrite grain boundaries. There is also growth of austenite into the ferrite grains. However, in the presence of 5 and 10% nitrogen in the shielding gas, the ferrite contents decreased to 35 and 29%, respectively. Figures 4 and 5 show the resultant microstructures. Both welds contained Widmanstätten austenite. Table 1 gives the chemical composition of the weld deposited in the presence of 5% nitrogen in the shielding gas. It was observed that due to loss of chromium during welding, the percentages of nickel and molybdenum contents in the weldments increased slightly as compared to those present in the parent metal and the filler wire. Autogenous bead-on-plate welding again resulted in higher amounts of ferrite in the weld. As shown in Fig. 6, the weld microstructure for autogenous GTA welding consisted of 64% ferrite with intragranular Widmanstätten austenite. Figures 7 and 8 show the weld micro-

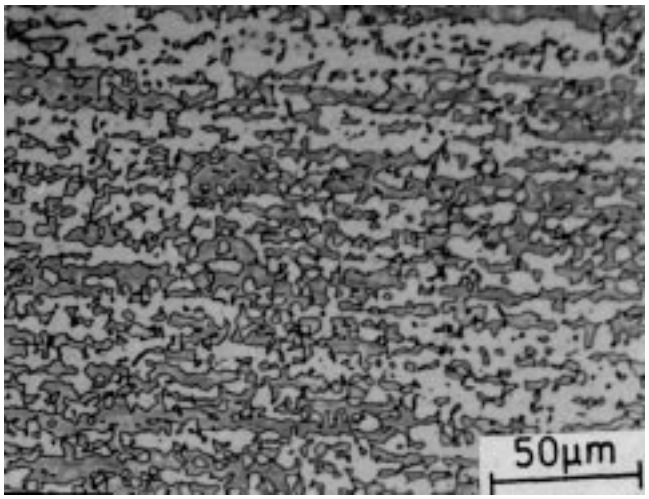


**Fig. 2** Microstructure of U-50. Etchant used: 40% KOH, 6 V

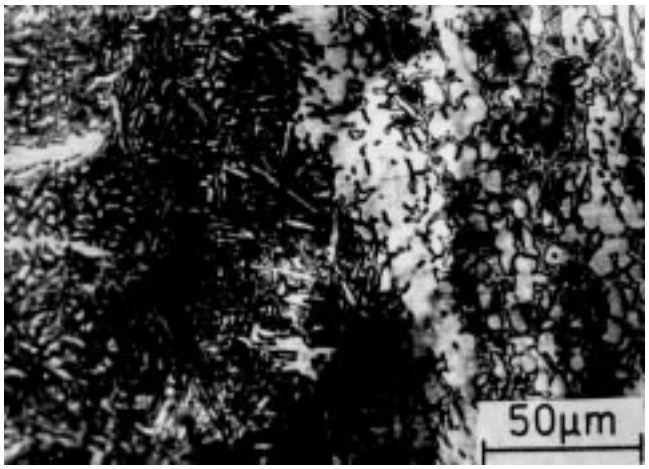


**Fig. 4** Gas tungsten arc weldment and heat affected zone (pure argon and 5% $N_2$)

structures obtained in microplasma and electron beam welding, respectively, which contained 73 and 77% ferrite.

### *3.2 Pitting Corrosion*

Table 4 gives the results obtained in the pitting corrosion tests in 6% $FeCl_3$ solutions. Here the loss in weights of the samples due to corrosion has been expressed in terms of corrosion rate in mils per year (mpy).

The use of nitrogen in the shielding gas during GTA welding with filler metal resulted in the decrease in corrosion rate from 378 mpy without nitrogen to 313 mpy with 10% nitrogen in the shielding gas. Visual and microscopic examinations indicated that weldments made in the nitrogen containing shielding gas had not experienced pitting attack on exposure to 6% $FeCl_3$ solution at 30 °C for 24 h. However, weldments made in pure argon as the shielding gas underwent pitting corrosion under identical conditions of testing. Most of the pits in the parent

**Table 4 Corrosion rates of U-50 weldments in 6% $FeCl_3$ solution (ASTM G 48 tests)**

| Weldments | Area of sample exposed, $mm^2$ | Welded area exposed, $mm^2$ | Weight loss, g | Corrosion rate, mpy | Attack in |
|---|---|---|---|---|---|
| **Gas tungsten arc welds** | | | | | |
| Pure Ar (F-22-8-3L) | 927 | 96 | 0.19 | 378 | Weld, HAZ, and parent |
| 5%$N_2$-95%Ar (F-22-8-3L) | 750 | 96 | 0.13 | 320 | HAZ and parent |
| 10%$N_2$-90%Ar (F-22-8-3L) | 824 | 96 | 0.14 | 313 | HAZ and parent |
| **Autogenous bead-on-plate** | | | | | |
| Gas tungsten arc | 870 | 45 | 0.022 | 46.7 | HAZ and parent |
| Microplasma | 834 | 27 | 0.035 | 77.4 | Weld and parent |
| Electron beam welding | 846 | 18 | 0.048 | 104.7 | Weld and parent |

HAZ, heat-affected zone

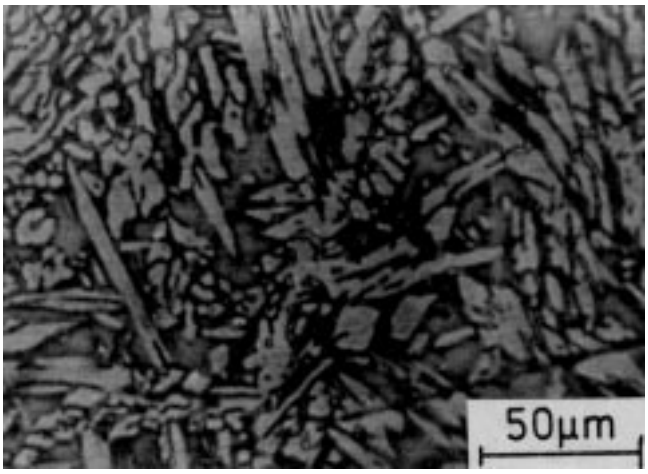


**Fig. 5** Gas tungsten arc weldment (pure argon and 10% $N_2$)

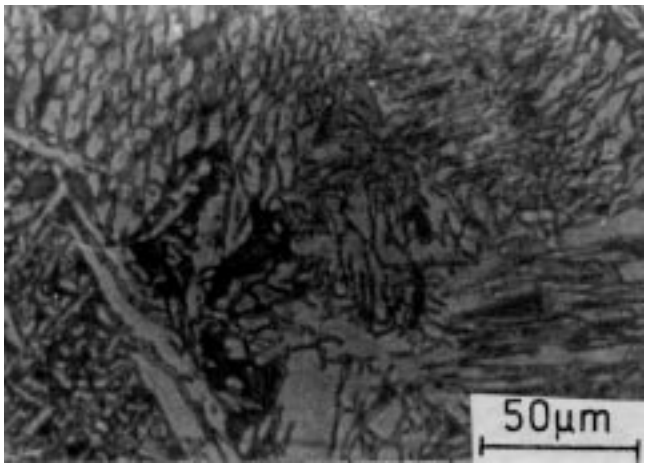


**Fig. 6** Autogenous gas tungsten arc weldment

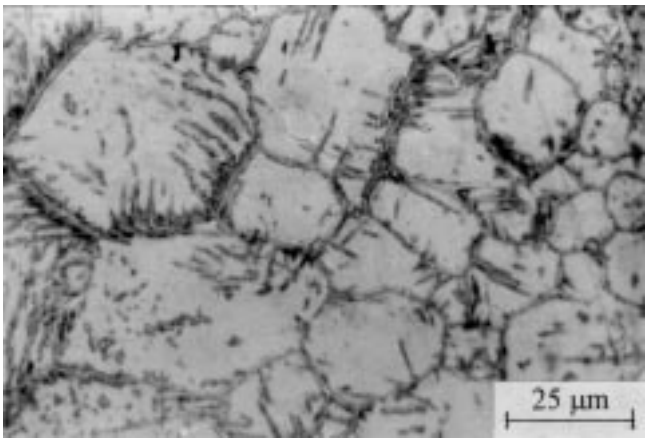


**Fig. 7** Microplasma weldment

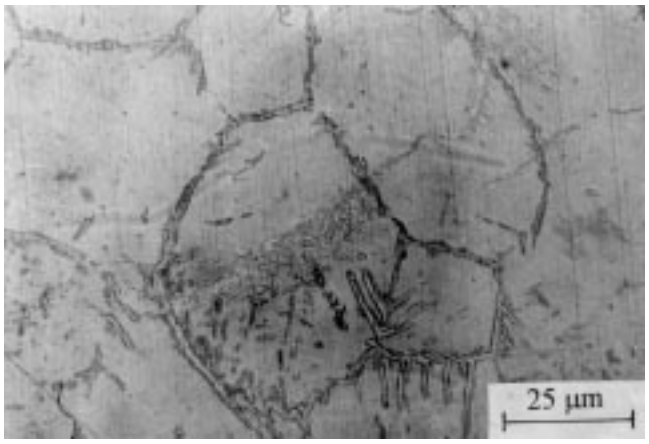


**Fig. 8** Weldment produced by electron beam welding

metal were covered with a surface film. Figure 9 shows a region in the parent metal containing a pit. The pit was not visible after the test. Light polishing on a cloth containing diamond paste revealed the pit beneath the surface film; part of the pit is still visible at the middle of the photograph. Selective attack of a phase, most probably austenite, was noticed inside the pits, as shown in Fig. 10. A similar type of corrosion was also observed for bead-on-plate autogenous GTA welds. However, the corrosion rate of these weldments was the lowest, 46.7 mpy, among all other welds studied in this investigation. Bead-on-plate microplasma and EBW resulted in pitting corrosion of the weld, HAZ, and the parent metal, though the corrosion rates associated with these welding procedures were quite low as compared to those obtained with the GTA welds in which filler metals were used along with shielding gases.

Anodic polarization in chloride-containing environments particularly in dilute solutions (0.005 and 0.01 *M* NaCl) indicated a distinct advantage of using nitrogen in the shielding gas. However, in a slightly concentrated NaCl solution (0.05 *M*), the advantage of nitrogen in the shielding gas became less pronounced. Table 5 gives the pitting potentials of these samples containing the weldments. It can be seen that use of 5 and 10% nitrogen in the shielding gas led to the increase in pitting potentials as compared to the pitting potentials of weldments made in argon in the same solution. In the former cases, there was no pitting in the welds; whereas in the later case all three regions, the welds, the HAZ, and the parent metal, showed the presence of pits.

For the bead-on-plate welds, there was not much difference in pitting potentials, as shown in Table 5. Pitting potentials of these welds were in the range of 400 to 500 mV in solutions containing 0.05 *M* Cl ions. As compared to the nitrogen containing GTA welds, these welds showed better resistance to pitting corrosion. The probable reason for this is discussed in a following section.

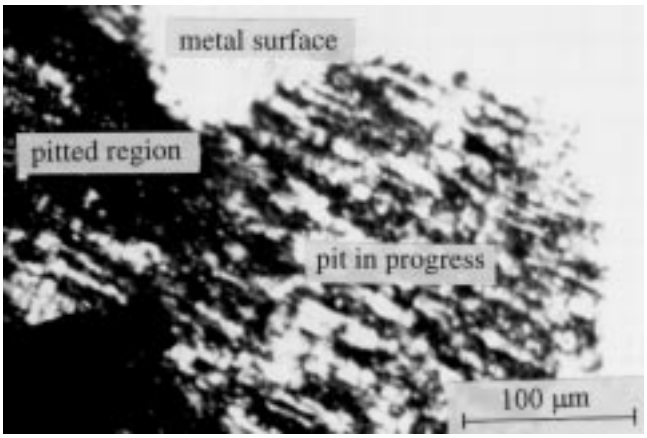


**Fig. 9** A pit in the parent metal, partially covered with surface film

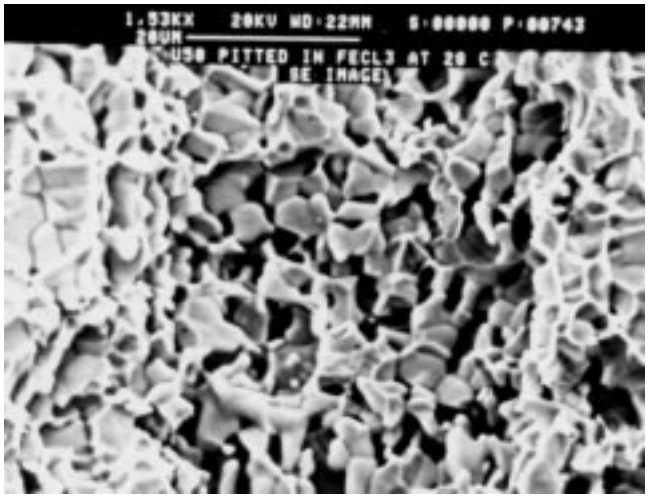

**Fig. 10** Scanning electron micrograph showing selective dissolution of a phase inside a pit

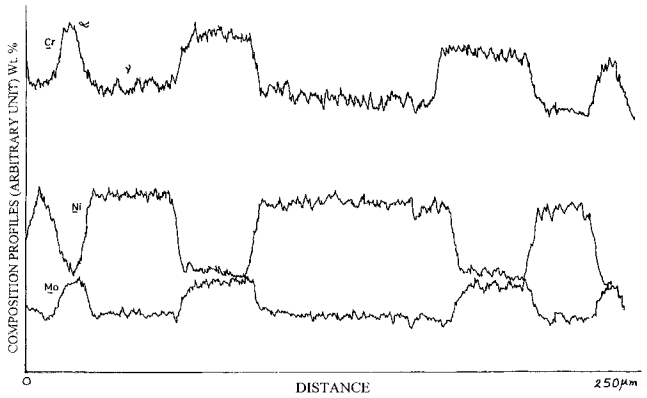


**(a)**

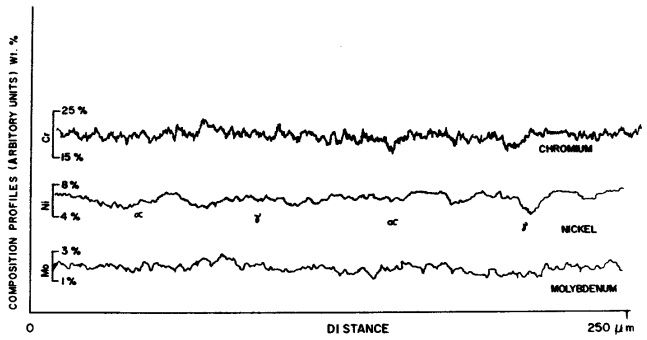


**(b)**

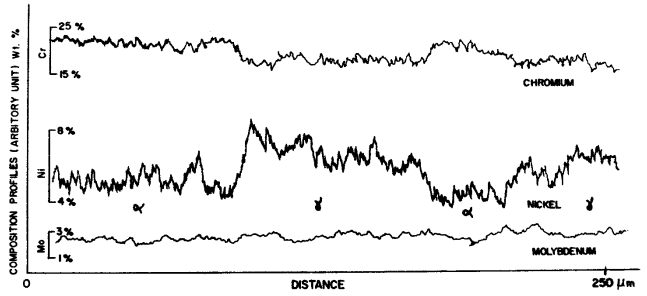


**(c)**

**Fig. 11** Electron probe microanalyses for chromium, nickel, and molybdenum in U-50 weldments made using (a) pure argon, ( b) argon and 10% nitrogen, and (c) microplasma

**Table 5 Pitting potentials of U-50 welds in NaCl solutions**

| | Pitting potentials, mV, SCE | | | | | |
|---|---|---|---|---|---|---|
| | U-50 (F-22-8-3L) | | | U-50 bead-on-plate | | |
| Solutions | Pure Ar | 5%N-95%Ar | 10%N-90%Ar | Gas tungsten arc | Microplasma | Electron beam weld |
| 0.005 *M* | 150 | 400 | 400 | … | … | … |
| 0.01 *M* | 140 | 350 | 375 | … | … | … |
| 0.05 *M* | 80 | 100 | 200 | 500 | 500 | 400 |

To find the distribution of chromium, nickel, and molybdenum in the austenite and ferrite phases present in the welds, electron probe microanalyses were carried out with three weldments, two of them were GTA weldments, one made using only argon, another made using argon plus 10% nitrogen, and the third made using microplasma. Beam size of EPMA is only 1.4 μm, and the analysis was carried out by profile scan technique in the steps of 5 μm, small enough to differentiate ferrite from austenite. Figure 11(a) to (c) shows the qualitative nature of the chromium, nickel, and molybdenum distributions in these weldments. There has been segregation of chromium and molybdenum in the ferrite phases and nickel in the austenite phases in GTA weldments made using only argon (Fig. 11a), whereas chromium and nickel were uniformly distributed in the weldments when 10% nitrogen was added to the shielding gas (Fig. 11b). Some amount of segregation of chromium and nickel in the ferrite and austenite phases respectively was noticed in the microplasma weldments (Fig. 11c). The distribution of molybdenum was observed to be more or less uniform in the microplasma weldments as well as in the GTA weldments in the presence of nitrogen.

## 4. Discussion

The solidification in duplex stainless steel welds occurs entirely through ferrite, with an austenite phase forming through a solid-state phase transformation process during post-solidification cooling. Thus, the as-solidified microstructure of the fusion zone consists of coarse, epitaxial ferrite grains with intergranular and intragranular austenite, although the formation, morphology, and resultant content of austenite are affected by weld compositions and welding parameters. Because the transformation occurs preferentially at prior ferrite grain boundaries, the intergranular austenite generally results in continuous networks at the ferrite grain boundaries, while intragranular austenite exhibits either Widmanstätten morphology or fine acicular morphology. The adverse effect of such weld microstructures on the localized corrosion resistance in chloride environments has been pointed out by various investigations (Ref 6). Hence more attention has been given to the localized corrosion behavior of the welds, related to their microstructural characteristics as well as composition.

Addition of nitrogen into the alloy certainly results in considerable beneficial influence on the weld pitting corrosion resistance (Ref 12). Intergranular austenite has been often observed to impede the pit propagation within ferrite in nitrogen enriched welds, whereas it served as a preferential site of pitting in low-nitrogen welds. Increased austenite with higher nitrogen improved the weld pitting corrosion resistance. However, part of the nitrogen present in the metal may be lost during welding; this may lead to loss of corrosion resistance. Blom (Ref 13) studied the effect of 10% $N_2$ in the shielding gas, argon, on the pitting resistance of duplex stainless steel weldments. There was significant reduction in pitting resistance of these weldments concurrent with the loss of nitrogen.

In the present investigation, nitrogen in the shielding gas was observed not only to modify the microstructure, but also to improve the pitting corrosion resistance of U-50 in $FeCl_3$ and NaCl solutions. This improvement in corrosion resistance is supposed to be due to the presence of a sufficient amount of nitrogen in the austenite, thus increasing its pitting corrosion resistance. Use of nitrogen in the shielding gas also resulted in uniform distribution of chromium and nickel in the ferrite and austenite phases and in higher amounts of austenite in the weld, which led to increased weldability. In the absence of nitrogen in the shielding gas, austenite was present in the microstructure in the form of a network around the ferrite grain boundaries, whereas with the addition of nitrogen, a good amount of austenite was obtained as intragranular Widmanstätten configuration. Electron probe microanalysis showed even distribution of chromium in the two phases, austenite and ferrite, in the presence of nitrogen. Thus chromium also helped in imparting corrosion resistance to both the phases, without being segregated to one of the phases, mostly in the ferrite phases due to its ferrite forming tendency.

Development of a proper microstructure is crucial to corrosion resistance of duplex stainless steel welds. Pitting corrosion within ferrite in the weld metals has been reported by many workers (Ref 6) who believed this to be due to chromium depletion arising from the precipitation of chromium carbide, chromium nitride, carbonitride, and other associated phases. However, no such attack was observed in the present investigation as the welds were free from corrosion. The pitting attack was confined to the base metal and heat affected zones. Presence of nitrogen increased the corrosion resistance not only of the austenite phase, but also of the ferrite phase. This may be due to reduction in the precipitation kinetics in the ferrite phase by nitrogen. Lardon et al. (Ref 14) observed reduction in the carbide precipitation kinetics in the ferrite phase due to the presence of nitrogen.

The bead-on-plate weldings resulted in low corrosion rates. This was attributed to the low heat input as well as smaller widths of welds and HAZs associated with these weldings. However, the welds produced by the microplasma and electron beam welding were seen to be sensitive to pitting attack. This could be due to the compositional differences in the two constituent phases, ferrite and austenite, as represented in Fig. 11(c), which shows depletion of chromium in the austenite phase. The autogenous GTA welds had pitting potential similar

to microplasma and electron beam welds. The heat input in case of these welds was lower than that associated with microplasma and electron beam weldings. However, it has been reported (Ref 15, 16) that the actual heat input and weld metal cooling rate also depend on electrode diameter, power supply polarity, shielding gas, and metal plate thickness. Thus the actual heat input and weld metal cooling rate probably resulted in the development of an optimum weld composition that had pitting resistance similar to microplasma and electron beam welds.

## 5. Conclusions

The following conclusions can be drawn:

- The presence of nitrogen in the shielding gas modified the weld microstructures with increased austenite contents.
- Gas tungsten arc welding with nitrogen in the shielding gas resulted in better pitting corrosion resistance of weldments and even distribution of chromium, nickel, and molybdenum in the austenite and ferrite phases. However, in the case of autogenous bead-on-plate GTA, weld resistance to pitting attack of the weld was not affected adversely even in the absence of nitrogen in the shielding gas.
- Microplasma and electron beam welding led to weldments with low corrosion rates. However, due to nonuniform distribution of alloying elements, particularly chromium, pitting attack was noticed in these welds.

### Acknowledgment

The authors are grateful to Dr. S. Banerjee, Associate Director, Materials Group and Head, Materials Science Division, and Mr. D.S.C. Purushotham, Director, Nuclear Fuels Group and Head, Radio Metallurgy Division, Bhabha Atomic Research Centre, Trombay, Mumbai, for their keen interest and encouragement during the course of this investigation.

### References

1. J.C. Lippold, W.A. Baselack, and L. Varol, Heat Affected Zone Liquation Cracking in Austenitic and Duplex Stainless Steels, *Weld. J.*, Vol 71 (No. 1), 1992, p 1s-14s
2. L.S. Redmerski, J.J. Eckenrod, and C.W. Kovach, Crevice Corrosion of Stainless Steel Welds in Chloride Environments, *Mater. Perform.*, Vol 22 (No. 6), 1983, p 31-39
3. E. Angelini and F. Zucchi, Corrosion Behaviour of Various Duplex Stainless Steels in Welded Condition, *Br. Corr. J.*, Vol 21 (No. 4), 1986, p 257-263
4. J. Pleva and S. Nordin, Properties of Different MMA-Welds on Modified 329 Ferritic-Austenitic Stainless Steel, *Duplex Stainless Steels*, R.A. Lula, Ed., American Society for Metals, 1983, p 603-629
5. H. Miyuki, T. Kudo, M. Koso, M. Miura, and T. Moroishi, 25% Chromium Containing Duplex Phase Stainless Steel for Hot Sea Water Application, *Duplex Stainless Steels*, R.A. Lula, Ed., American Society for Metals, 1983, p 95-112
6. N. Sridhar, L.H. Flashe, and J. Kolts, Effect of Welding Parameters on Localized Corrosion of a Duplex Stainless Steel, *Mater. Perform.*, Vol 23 (No. 12), 1984, p 52-55
7. T. Ogawa and T. Koseki, Effect of Composition on Metallurgy and Corrosion Behavior of Duplex Stainless Steel Weld Metals, *Weld. J.*, 1989, p 181s-191s
8. R.A. Little, *Welding and Welding Technology*, McGraw-Hill, 1985, p 203
9. A.R. George and B.G. Russell, How Accurate Are Methods for Measuring Ferrite?, *Met. Prog.*, Vol 111 (No.1), 1969, p 76
10. E. Stalmasek, Measuring Ferrite Content in Austenitic Stainless Steels, *WRC Bull.*, Vol 318, 1986, p 11W
11. T.R.G. Kutty, K.N. Chandrasekharan, P. Panakkal, S.K. Ghosal, and P.K. De, Use of Ultrasonic Velocity for Nondestructive Evaluation of Ferrite Content in Duplex Stainless Steels, *NDT Int.*, Vol 20 (No. 6), 1989, p 359-363
12. M. Liljas and R. Qvarfort, Influence of Nitrogen on Weldments in UNS S31803, *Duplex Stainless Steel*, R.A. Lula, Ed., American Society for Metals, 1983, p 244-256
13. K.J. Blom, Improving Properties of Weld Joints in Duplex Stainless Steel by Welding with Shielding Gas Containing Nitrogen, *Stainless Steels*, University of York, London, 1987, p 12-125
14. J.M. Lardon, J. Charles, F. Dupoiron, P. Pugeault, and D. Catelin, Duplex Stainless Steel as Modern Material: Corrosion Resistance of Base Metal and Welded Joints, *Stainless Steels*, University of York, London, 1987, p 422-431
15. B.L. Shultz and C.E. Jackson, *Weld. J.*, Research Supplement, Vol 52 (No. 1), 1973, p 26-S
16. W.E. Lukens and R.A. Morris, *Weld. J.*, Vol 61 (No. 1), 1982, p 27